J Therm Anal Calorim
DOI 10.1007/s10973-016-5805-z

Experimental investigations of thermal stability of some morpholinecarbamic acid complexes of copper(II) and zinc(II)

Shashi B. Kalia[1] · Rajesh Kumar[1] · Monika Bharti[1] · J. Christopher[2]

Received: 17 July 2015 / Accepted: 29 August 2016

Abstract Some new carbamates, viz. $M(MorphcbmH)_2X_2$ (MorphcbmH = morpholinecarbamic acid, M = Cu, X = Cl, ClO_4,NO_3; M = Zn, X = Cl, ClO_4, NO_3, CH_3COO and $X_2 = SO_4$), have been synthesized and investigated. Compounds were characterized by elemental analysis, molar conductance, FT infrared, fluorescence, NMR (^1H and ^{13}C) and solution electronic absorption spectral studies. Room temperature field-dependent magnetic susceptibility measurements, PXRD spectral and cyclic voltametric studies were also conducted. Chelating bidentate mode of coordination of ligand, MorphcbmH with four coordination around metal ion has been proposed. Ligand and its compounds have also been studied using non-isothermal thermogravimetric analysis and differential scanning calorimetric analytical techniques which inferred formation of metal oxide/MCO_3 as final thermal decomposition products. Compounds were screened against the lipase enzyme for assaying their enzyme activity and were found to retard the lipase activity from 48.16 to 0.044 μmol mL^{-1} min^{-1}.

Keywords Morpholinecarbamic acid (MorphcbmH) · Copper(II) · Zinc(II) · TG/DSC · Fluorescence spectroscopy · Cyclic voltammetry

Introduction

Carbamate compounds with general formula $^{-}O_2CNR_2$, R being H, an alkyl or an aryl group are of particular interest due to their applications in polymer industry [1–3], as agrochemicals [1–5] and pharmaceuticals [1–3]. Decomposition of carbamates has been reported to be a fairly slow process, and to speed up the reaction, use of catalysts has been proposed. Generally, carbamates thermally decompose to give various products such as amine, alkene, carbon dioxide, alcohol and isocyanate depending upon their alkyl/aryl ester derivative carbamate [6, 7]. However, thermal investigations on metal carbamates are scanty [8]. Since carbamate compounds have insecticidal applications and are less toxic and are biodegradable in nature, it becomes important to study their thermal stability for accounting nature of residues in environment particularly in soil and water bodies. In view of this, thermogravimetric (TG) and differential scanning calorimetric (DSC) analytical techniques have been used to investigate thermal stability and decomposition patterns of free ligand, morpholinecarbamic acid (MorphcbmH) and some of its complexes.

Experimental

Materials

All the chemicals used were purchased from Fluka and without further purification.

✉ Shashi B. Kalia
shashibalakalia@rediffmail.com

[1] Department of Chemistry, Himachal Pradesh University, Shimla 171005, India

[2] Indian Oil Corporation, R&D, Faridabad, Haryana, India

Synthesis of ligand and complexes

MorphcbmH

Dry carbon dioxide gas was passed for about 5 min through continuously stirred solution of morpholine (1 ml, 1000 μl) in hexane (3–5 ml). White-colored product separated out immediately. It was filtered, washed with hexane, dried in air and finally in a calcium chloride desiccator.

Cu(MorphcbmH)$_2$X$_2$ ((M = Cu, X = Cl, ClO$_4$,NO$_3$) and Zn(MorphcbmH)$_2$X$_2$ (X = Cl, ClO$_4$, NO$_3$, CH$_3$COO and X$_2$ = SO$_4$)

$CuX_2 \cdot xH_2O$, 0.382 mmol (65.06 mg for X = Cl, $x = 2$; 92.21 mg for X = NO_3, $x = 3$ and 141.22 mg for X = ClO_4, $x = 6$) and $ZnX_2 \cdot xH_2O$, 0.382 mmol (52.01 mg for X = Cl, $x = 0$; 141.62 mg for X = ClO_4, $x = 6$; 72.13 mg for X = NO_3, $x = 0$; 75.44 mg for X = CH_3COO, $x = 1$ and 109.75 mg for X = SO_4, $x = 7$) were dissolved in ethanol (5 ml). To this solution was added solid morpholinecarbamic acid (100 mg, 0.764 mmol,) in small portions (10 mg) with stirring after successive intervals of 15–20 min in a total period of about 3 h. The reaction was carried out at room temperature (25–30 °C). Complex separates out within an hour after addition of complete acid, yet reaction mixture was stirred for another 2–3 h to ensure completion of reaction. The solid product (for copper compounds, yellow when X = Cl, sky blue when X = NO_3 and bluish green when X = ClO_4 and for zinc compounds, white when X = Cl, ClO_4, NO_3, CH_3COO and $X_2 = SO_4$) was then centrifuged, washed with ethanol using centrifugation technique and dried in air. Final drying was done in a calcium chloride desiccator.

Analysis and techniques

Carbon, hydrogen, nitrogen and sulfur analyses were performed using Elemental Analyzer Vario EL-III. Copper and zinc were determined volumetrically by EDTA using Pyrocatechol violet and Eriochrome Black T (EBT) as indicators, respectively.

MorphcbmH Analysis found: C 45.84, H 6.90, N 10.72 %; Calculated for $C_5H_9NO_3$: C 45.80, H 6.87, N 10.68 %. Reaction yield 96 %. Decomposition temperature: 65 °C.

Cu(MorphcbmH)$_2$Cl$_2$ Analysis found: C 30.30, H 4.49, N 7.10, Cu 15.98, Cl 17.92 %; Calculated for $CuC_{10}H_{18}N_2O_6Cl_2$: C 30.26, H 4.53, N 7.06, Cu 16.01, Cl 17.90 %. Reaction yield 90 %. Decomposition temperature: 110 °C.

Cu(MorphcbmH)$_2$(ClO$_4$)$_2$ Analysis found: C 22.90, H 3.45, N 5.35, Cu 12.12, Cl 13.55 %; Calculated for $CuC_{10}H_{18}N_2O_{14}Cl_2$: C 22.87, H 3.43, N 5.33, Cu 12.10, Cl 13.53 %. Reaction yield 89 %. Decomposition temperature: 142 °C.

Cu(MorphcbmH)$_2$(NO$_3$)$_2$ Analysis found: C 26.72, H 4.02, N 12.47, Cu 14.10 %; Calculated for $CuC_{10}H_{18}N_4O_{12}$: C 26.69, H 4.00, N 12.45, Cu 14.12 %. Reaction yield 91 %. Decomposition temperature: 142 °C.

Zn(MorphcbmH)$_2$Cl$_2$ Analysis found: C 30.18, H 4.50, N 7.06, Zn 16.30, Cl 17.80 %; Calculated for $ZnC_{10}H_{18}N_2O_6Cl_2$: C 30.15, H 4.52, N 7.03, Zn 16.33, Cl 17.83 %. Reaction yield 88 %. Decomposition temperature: 165 °C.

Zn(MorphcbmH)$_2$(ClO$_4$)$_2$ Analysis found: C 22.85, H 3.45, N 5.30, Zn 12.31, Cl 13.45 %; Calculated for $ZnC_{10}H_{18}N_2O_{14}Cl_2$: C 22.81, H 3.42, N 5.32, Zn 12.35, Cl 13.49 %. Reaction yield 90 %. Decomposition temperature: 136 °C.

Zn(MorphcbmH)$_2$(NO$_3$)$_2$ Analysis found: C 26.55, H 3.97, N 12.40, Zn 14.45 %; Calculated for $ZnC_{10}H_{18}N_4O_{12}$: C 26.60, H 3.99, N 12.41, Zn 14.41 % Reaction yield 91 %. Decomposition temperature: 154 °C.

Zn(MorphcbmH)$_2$(CH$_3$COO)$_2$ Analysis found: C 37.78, H 5.40, N 6.31, Zn 14.62, CH$_3$COO 26.55 %; Calculated for $ZnC_{14}H_{24}N_2O_{10}$: C 37.75, H 5.39, N 6.29, Zn 14.60, CH$_3$COO 26.51 % Reaction yield 90 %. Decomposition temperature: 147 °C.

Zn(MorphcbmH)$_2$SO$_4$ Analysis found: C 28.40, H 4.22, N 6.63, S 7.58, Zn 15.34 %; Calculated for $ZnC_{10}H_{18}N_2SO_{10}$: C 28.36, H 4.25, N 6.61, S 7.56, Zn 15.36 % Reaction yield 85 %. Decomposition temperature: 152 °C.

Physical measurements

Room temperature molar conductance measurements (10^{-3} M DMSO solutions) were taken by using Elico conductivity bridge type CM-82T. Thermal analyses of the complexes were carried out by using thermogravimetric analyzer (TGA)-Model 2950 and differential scanning calorimeter (DSC)-Model 2920, Make-TA Instruments, USA. Thermocouple Pt/Pt–Rh (10 %) with temperature range of 20–800 °C was employed. Sample (5–10 mg) in a Pt crucible under static air atmosphere was heated at a rate of 10 °C min^{-1}. TGA instrument was calibrated periodically using Al_2O_3 as standard reference. Nicolet 5700 FTIR spectrophotometer was used to record infrared spectra of complexes as KBr pellets in 4000–600 cm^{-1} region and as NaCl plates as windows in region 600–200 cm^{-1}. Perkin Elmer LS 55 spectrometer with scanning range 200–900 nm was used to measure fluorescence emission spectra of compounds (10^{-3} M DMSO solution). ^{1}H NMR spectra of complexes were recorded on JEOL JNM PMX60 SI/DRX-300 MHz Bruker spectrophotometers using $(CD_3)_2SO$ as solvent and TMS as an internal standard, while ^{13}C NMR spectra were recorded on DRX-300 MHz Bruker spectrophotometer using same solvent. Magnetic susceptibilities of the samples were measured on vibrating sample magnetometer PAR-155 (model-152). The instrument was calibrated with $Cu(OOCCH_3)_2 \cdot H_2O$, whose magnetic susceptibility at room temperature is known. Cary

100 Bio UV–Visible recording Spectrophotometer (range 200–900 nm) was used to record solution (DMSO) electronic absorption spectra of complexes, with solvent as reference, in quartz glass cells. PXRD patterns were obtained using Bruker AXSd8 advance X-ray diffractometer with Mo-K_α ($\lambda = 0.7107$ Å) and Cu-K_α ($\lambda = 1.54184$ Å) radiation sources and [XPERT-PRO] diffractometer with Cu-K_α ($\lambda = 1.54184$ Å) radiation source. The measurements were taken at a temperature of 25 °C (RT) and a 2θ angle range of 10°–80°. A step resolution of 0.019° was used with a step time of 19.2 s. Cyclic voltammograms of compounds in DMSO solution (10^{-3} M) were recorded on Autolab Potentiostat 128 N Electrochemical Analyzer using KCl/$NaClO_4$ (10^{-1} M) as supporting electrolyte in the potential range −2 to +2 V at a scan rate of 100 mV s^{-1}.

Lipase enzyme activity

Compounds were also investigated for the lipase enzyme inhibition (steapsin) activity at different incubation times, i.e., 10, 30, 50 and 70 min along with control. Experiments were performed in triplicate. In six dry and clean test tubes labeled A, B, C, D, E and F, tris buffer gum acacia solution (2.90 mL, 0.05 M, pH 8.5) was taken. These were incubated in water bath at 45 °C for 10 min, removed from the water bath and cooled to room temperature. Eighty microliter (80 μl) of p-nitrophenylpalmitate (p-NPP) substrate solution was added to each test tube which was again incubated in water bath at 45 °C for another 10 min. In another set of four clean and dry test tubes was taken 1 mg of solid compound under study and added 10 μl of steapsin lipase enzyme in each of these test tubes. The test tubes were numbered as 1, 2, 3 and 4 and were incubated at 45 °C on water bath for 10, 30, 50 and 70 min, respectively. All the experiments were performed in triplicate. In another one clean and dry test tube, 10 μl of steapsin lipase enzyme was taken and to it added the solution of test tube marked A. Then, again incubated the test tube in water bath at 45 °C for 10 min. The enzyme activity was arrested by keeping the reaction mixture at −80 °C for about 5 min. Then, A_{410} nm of the solution was measured. Added the solutions of test tubes B, C, D, E into test tubes 1, 2, 3, 4 after 10, 30, 50 and 70 min, respectively. Test tubes were incubated in water bath at 45 °C for 10 min. The enzyme activity was arrested by keeping the reaction mixture at −80 °C for about 5 min. Then, A_{410} of the solution was measured. The activity of enzyme was calculated with the help of formula.

$$\begin{aligned}\text{Activity of enzyme} = {} & \frac{\text{Test(t)} - \text{Control(C)}}{\text{OD of Standard}} \\ & \times \text{Conc. of standard} \times \frac{1}{10} \\ & \times \text{Dilution factor} \\ & \times \frac{1}{\text{Molecular weight of p} - \text{NPP}}\end{aligned}$$

Results and discussion

Free ligand, MorphcbmH (Eq. 1) and its copper(II) and zinc(II) complexes were synthesized according to the reaction (Eq. 2):

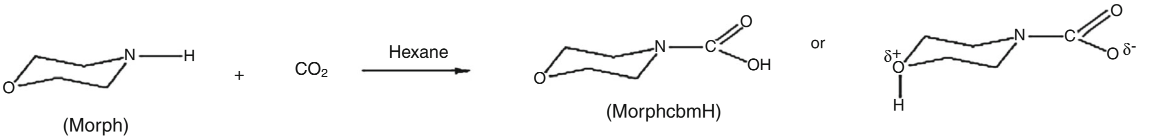

(1)

Synthesis of 4-MorphcbmH

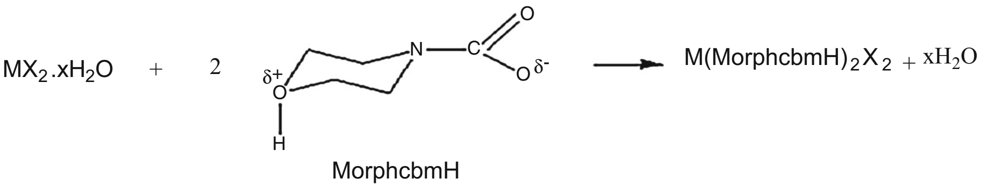

(2)

Synthesis of metal complexes

where (M = Cu, X = Cl, $x = 2$; X = NO_3, $x = 3$ and X = ClO_4, $x = 6$ and M = Zn, X = Cl, NO_3 and $x = 0$; X = ClO_4, $x = 6$; X = CH_3COO, $x = 1$ and $X_2 = SO_4$, $x = 7$)

These complexes do not melt but decompose between 110 and 165 °C and are sparingly soluble in methanol but are fairly soluble in DMSO.

Molar conductance studies

The 10^{-3} M DMSO solution of complexes M(MorphcbmH)$_2$X$_2$ (M = Cu, X = Cl, ClO_4, NO_3; M = Zn, X = Cl, ClO_4, NO_3, CH_3COO) exhibited molar conductance values, 136–179 ohm^{-1}cm^2 mol^{-1} that supported their 1:2 electrolytic behavior [9], whereas Zn(MorphcbmH)$_2$SO$_4$ has molar conductance value 15 ohm^{-1} cm^2 mol^{-1} suggesting its non-electrolytic nature.

Infrared spectral studies

FTIR spectra of MorphcbmH and its complexes, viz. M(MorphcbmH)$_2$X$_2$ (M = Cu, X = Cl, ClO_4, NO_3; M = Zn, X = Cl, ClO_4, NO_3, CH_3COO and $X_2 = SO_4$), exhibit a new relatively broad and strong band at 3415–3431 cm^{-1} due to ν O–H stretching vibration that points to the formation of O–H bond supporting the presence of carbamate ligand as a Zwitterion. Observation of this band at higher wave number than the usual values of 3400–3200 cm^{-1} infers that interaction of lone electron pair on oxygen with positively charged hydrogen is stronger than normal O–H interaction. Peculiar infrared spectral absorptions in the regions 1570–1633 and 1544–1565 cm^{-1} due to ν(CO_2) and ν(C=N) corresponding to >NCO$_2$ moiety of MorphcbmH ligand and its complexes are informative of bridging bidentate binding mode of ligand in all metal-carbamic acid complexes under present investigations. This kind of binding is further supported by Calderazzo et al. [10]. Appearance of additional bands in the region 361–420 cm^{-1} due to ν(M–O) in complexes as compared to free carbamic acid ligand reveals the formation of metal–oxygen bond [11].

Fluorescence spectroscopy studies

The fluorescent spectra of MorphcbmH and its complexes exhibit maximum emission wavelengths ($\lambda_{\max}^{em}$) at 352 nm and 407–470 nm, respectively, corresponding to blue light emission, the excitation wavelength being 290 nm for ligand and 370 nm for all compounds. A red shift in emission peak $\lambda_{\max}^{em}$ values upon incorporation of metal ion into ligand moiety has been observed [12]. The fluorescent emission intensity (I_{em}) for free ligand MorphcbmH is 309 a.u. A dramatic decrease in emission intensities on complex formation for M(MorphcbmH)$_2$X$_2$ (M = Cu, X = Cl, ClO_4, NO_3; M = Zn, X = Cl, ClO_4, NO_3, and $X_2 = SO_4$) has been observed to fall at 47–230 a.u., whereas there is increase in emission intensity on complex formation for Zn(MorphcbmH)$_2$(CH_3COO)$_2$ lying at 330 a.u. Furthermore, an increase in excitation intensity (I_{ex}) for above complexes, i.e., 180–954 a.u. at $\lambda_{\max}^{ex} = 370$ nm, has been observed as compared to that for free ligand, i.e., MorphcbmH: $I_{ex} = 171$ a.u. at $\lambda_{\max}^{ex} = 290$ nm. Degree of fluorescence quenching increases upon complex formation with metal ions [13] and is explained by processes, magnetic perturbation, redox-activity, and electronic energy transfer.

^{1}H NMR spectra

^{1}H NMR spectra of MorphcbmH and Zn(MorphcbmH)$_2$X$_2$ (X = Cl and $X_2 = SO_4$) have also been performed. Heterocyclic secondary amine, i.e., Morph exhibits resonance signal due to O–H proton, δ 1.65; –CH$_2$– protons, 2,6- and 3,5-protons, δ 2.54–2.57 and δ 3.63–3.66; >N-CH$_3$ protons, δ nil ppm. ^{1}H NMR spectrum of free acid ligand, MorphcbmH (Fig. 1), shows the resonance signals as two triplets for 2,6 and 3,5-methylene protons: δ 2.91; δ 3.71.(Table 1). The signal due to >N–H proton of free Morph was not observed suggesting thereby formation of MorphcbmH ligand on reaction with carbon dioxide, while appearance of new signal at δ 3.44 ppm has been attributed to proton resonance of O–H as a result of formation of new O–H bond as shown below:

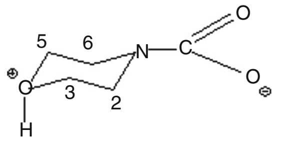

Zwitterionic form of MorphcbmH

Appearance of this downfield signal further suggests presence of positive charge on oxygen atom (deshielding the proton) as a result of proton binding with oxygen atom of O< group yielding Zwitterionic form of acid ligand.

For complexes, viz. Zn(MorphcbmH)$_2$X$_2$ (X = Cl and $X_2 = SO_4$) (Figs. 2, 3), separate triplets due to 2,6-methylene (δ 3.73 ppm) and (δ 3.50 ppm) and 3,5-methylene (δ 2.97 ppm), and (δ 2.81 ppm) protons have been observed on the downfield and upfield side, respectively, in comparison with corresponding free ligand (Table 1). Observation of single triplet instead of two

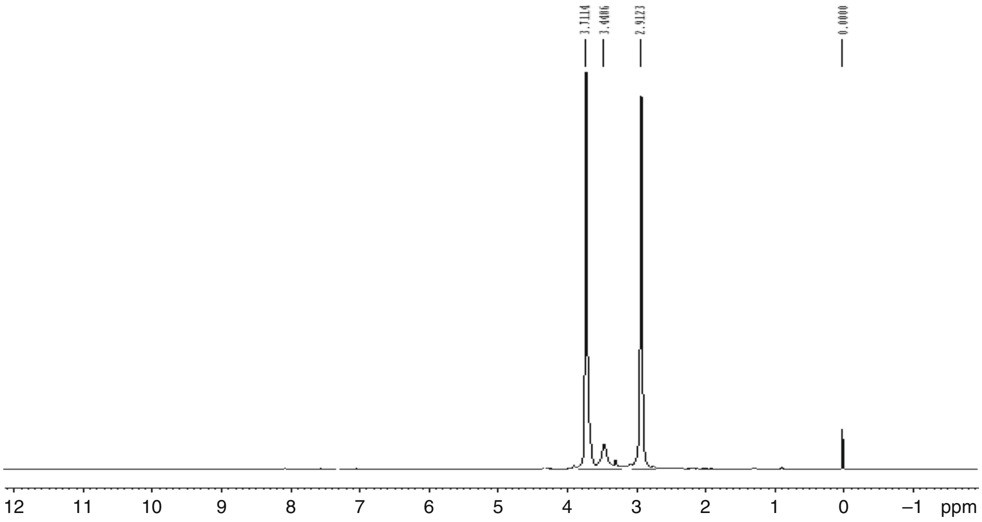

Fig. 1 ^{1}H NMR Spectrum of MorphcbmH

Table 1 ^{1}H NMR spectral data, δ (ppm) for Morph and MorphcbmH and its zinc(II) complexes

Sr. no.	Compound	NH/O–H	(2,6-) CH_2	(3,5-) CH_2
1.	Morph	1.65(s, 1H)	2.54–2.57 (t, 4H)	3.63–3.66(t, 4H)
2.	MorphcbmH	3.44(s, 1H)	2.91(t, 4H)	3.71(t, 4H)
3.	$Zn(MorphcbmH)_2Cl_2$	3.40(s, 1H)	3.73(t, 4H)	2.97(t, 4H)
4.	$Zn(MorphcbmH)_2SO_4$	3.30(s, 1H)	3.50(t, 4H)	2.81(t, 4H)

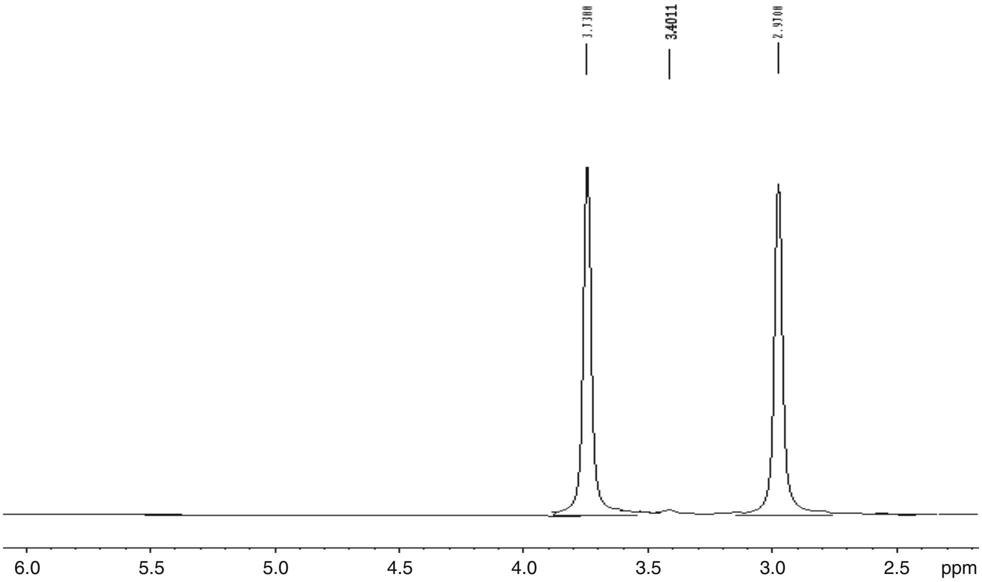

Fig. 2 ^{1}HNMR Spectrum of $Zn(MorphcbmH)_2Cl_2$

triplets for 2,6-methylene proton in all complexes under study in comparison with free acid ligand may result either because of hindered rotation of $O_2C{=}N$ group of MorphcbmH ligand or because of accidental degeneracy attributed to high local symmetry of NCO_2M moiety [11]. A direct relationship between $>NCO_2$ vibrational frequency and chemical shift values—deshielding of N-bonded methylene protons upon coordination through oxygen atoms to the central metal ion—has been observed, i.e., $Zn(MorphcbmH)_2Cl_2$ (ν $NCO_2 = 1621\ cm^{-1}$) $<$ $Zn(MorphcbmH)_2SO_4$ (ν $NCO_2 = 1625\ cm^{-1}$) [14, 15], δ 3.73 $>$ δ 3.50 ppm.

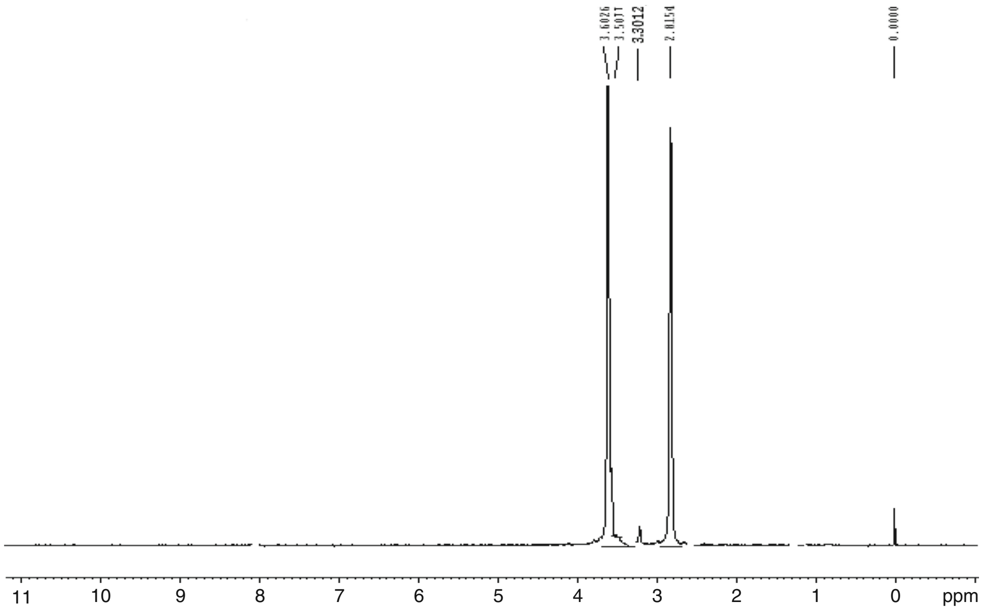

Fig. 3 ^{1}H NMR Spectrum of Zn(MorphcbmH)$_2$SO$_4$

^{13}C NMR spectra

^{13}C NMR spectrum of free ligand MorphcbmH (Fig. 4) shows signals: 2,6–CH$_2$, δ 76.75–77.39 ppm; 3,5 –CH$_2$, δ 67.02–67.62 ppm and >NCO$_2$, δ 170 ppm (Table 2). ^{13}C NMR spectra of zinc(II) complexes of MorphcbmH, viz. Zn(MorphcbmH)$_2$Cl$_2$ and Zn(MorphcbmH)$_2$SO$_4$, show (Figs. 5, 6) signals: 2,6 –CH$_2$, δ 77.93–78.59 and δ 78.06–78.71 ppm; 3,5 –CH$_2$, δ 70.75 and δ 67.06 ppm; >NCO$_2$, δ 172 and δ 180 ppm, respectively (Table 2).

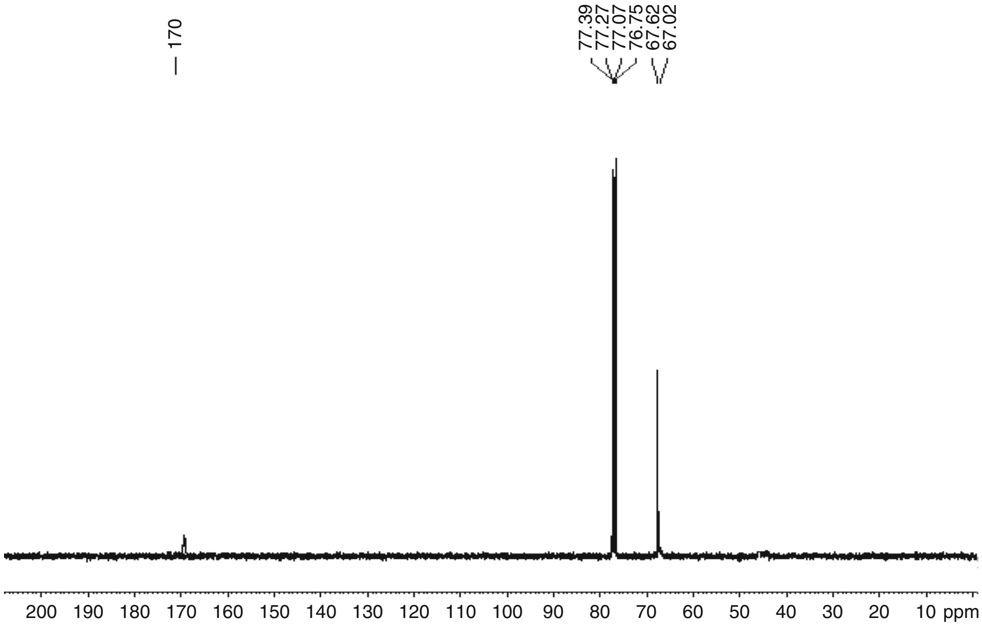

Fig. 4 ^{13}C NMR Spectrum of MorphcbmH

Table 2 ^{13}C NMR spectral data, δ (ppm) for MorphcbmH and its zinc(II) complexes

Sr. no.	Compound	(2,6-) CH$_2$	(3,5-) CH$_2$	>NCO$_2$
1.	MorphcbmH	76.75–77.39	67.02–67.62	170
2.	Zn(MorphcbmH)$_2$Cl$_2$	77.93–78.59	70.75	172
3.	Zn(MorphcbmH)$_2$SO$_4$	78.06–78.71	67.06	180

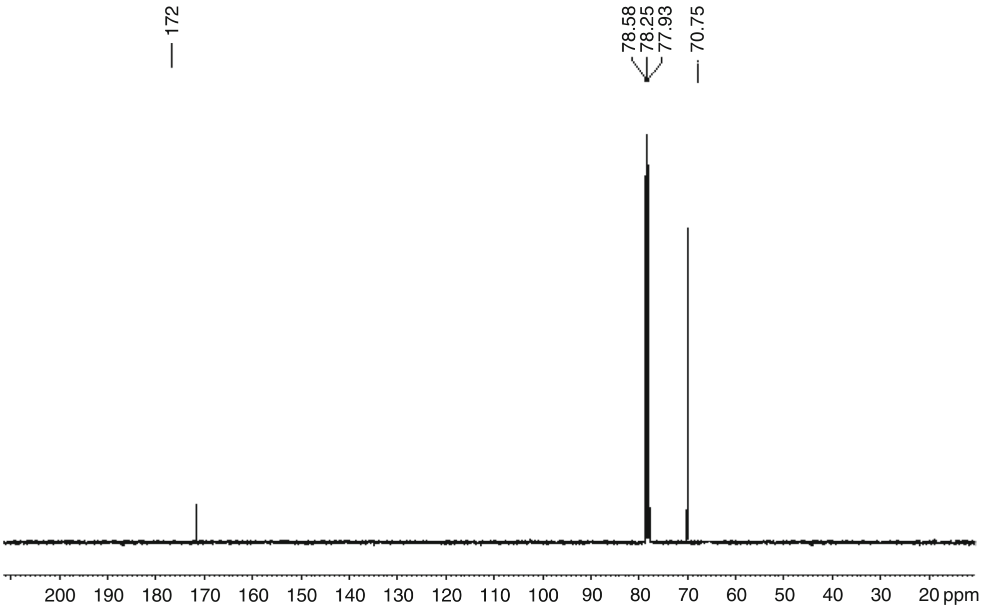

Fig. 5 ^{13}C NMR Spectrum of $Zn(MorphcbmH)_2Cl_2$

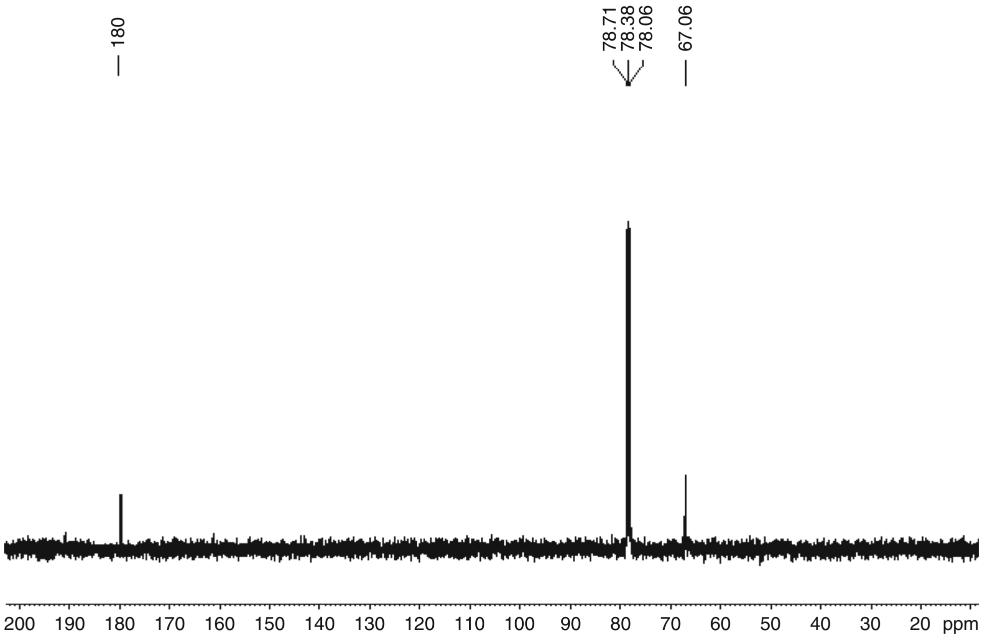

Fig. 6 ^{13}C NMR Spectrum of $Zn(MorphcbmH)_2SO_4$

That all ^{13}C δ values have been observed at higher numbers as compared to free ligand indicate greater deshielding of carbon atoms plausibly due to higher electronegativity of oxygen atom at 4th position of MorphcbmH ligand.

Magnetic study

For copper(II) complexes, viz. $Cu(MorphcbmH)_2X_2$ ($X = Cl, ClO_4, NO_3$) room temperature magnetic moment values, have been observed to lie in the range 2.40–1.79 B.M. indicative of the presence of one unpaired electron per copper(II) ion. Due to spin–orbit coupling, magnetic moment values are higher than the spin-only value. Room temperature variation of magnetization with field (−10,000 to 10,000 G) and observation of hysteresis loops for copper(II) complexes, viz. $Cu(MorphcbmH)_2X_2$ ($X = Cl, ClO_4, NO_3$), have revealed them to attain saturation magnetization in the applied field strength—typical of ferromagnetic materials. The values of magnetic parameters, i.e., M_S(saturation magnetization); H_C(coercivity); and M_R(remanence magnetization), calculated from the hysteresis loops lie in the range $1.9–25 \times 10^{-4}$ emu/g;

2600–5800 G; and 0.6–11 × 10^{-4} emu/g, respectively. Range of parameters is compatible with the literature data. Calculated M_R/M_S values for these complexes lie in the range 0.31–0.46. Higher the value of M_R/M_S ratio greater is the softness behavior of the substance [16]. Zinc(II) carbamate complexes $Zn(MorphcbmH)_2X_2$ (X = Cl, ClO_4, NO_3, CH_3COO and $X_2 = SO_4$,) exhibit room temperature magnetic moment values in the range 0.2–0.05 B.M. indicating their diamagnetic behavior.

Electronic spectra

Electronic absorption spectra of MorphcbmH complexes of copper(II), viz. $Cu(MorphcbmH)_2X_2$ (X = Cl, ClO_4, NO_3) in DMSO solution, exhibit two bands in the regions: Band I, 11,990–13,927 to 13,888–14,598 cm^{-1} is considered to contain electronic transitions $d_{xy} \rightarrow d_x^2 - {}_y^2$ and $(d_{xz}, d_{yz}) \rightarrow d_x^2 - {}_y^2$ for copper(II) ion in tetragonally distorted octahedral environments. Band II, 28,571–29,325 cm^{-1} is assigned to L → M charge transfer transition $2p_\pi \rightarrow (d_x^2 - {}_y^2)$. For zinc(II) complexes, viz. $Zn(MorphcbmH)_2X_2$ (X = Cl, ClO_4,NO_3,CH_3COO and $X_2 = SO_4$), electronic spectral bands have been observed to lie in the range, 27,173–28,735 cm^{-1}. On the basis of the literature reports, zinc(II) carbamate complexes can have dimeric structures as shown below (Scheme 1) with (ZnO_4X) (X = Cl, ClO_4, CH_3COO, NO_3) and ZnO_4X_2 ($X_2 = SO_4$) chromophores. Dimeric/tetrameric nature of complexes finds support from the literature due to Tang et al. [17].

X-ray diffraction studies

PXRD patterns of MorphcbmH and its complexes, viz. $Cu(MorphcbmH)_2Cl_2$, and $Zn(MorphcbmH)_2X_2$ (X = Cl, NO_3), exhibit sharp XRD peaks (Figs. 7, 8) with low value of full width at half maximum (FWHM) thus indicating their crystalline nature [18, 19]. By using Debye–Scherrer equation [18, 19], XRD crystallite sizes corresponding to a value of full width at half maximum (FWHM) for six peaks of high intensity at respective θ values were calculated. Tables 3 and 5 show the d spacing, 2θ, relative intensity, FWHM and crystallite size of these complexes. The mean particle sizes calculated using the Debye–Scherrer equation from the line broadening in the diffractograms are found to be 10.43 and 8.97, 8.88, and 103.21 nm for free ligand MorphcbmH and $Cu(MorphcbmH)_2Cl_2$, $Zn(MorphcbmH)_2Cl_2$, and $Zn(MorphcbmH)_2(NO_3)_2$ complexes, respectively. The data (Tables 3–5) show that larger the crystallite size of the sample, the sharper is the peak, i.e. decrease in FWHM on the XRD pattern. The tabular data for copper(II) complexes of MorphcbmH is in good agreement with that for the reported crystalline complexes, carbamates and agriculturally active organic compounds [20] (Table 4).

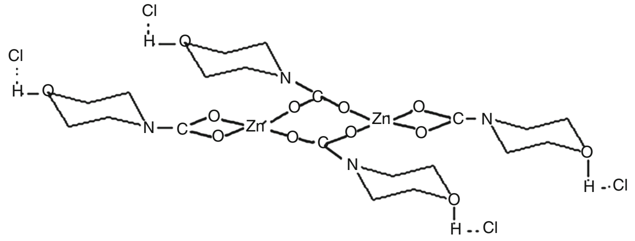

Scheme 1 Proposed structure of $Zn(MorphcbmH)_2Cl_2$

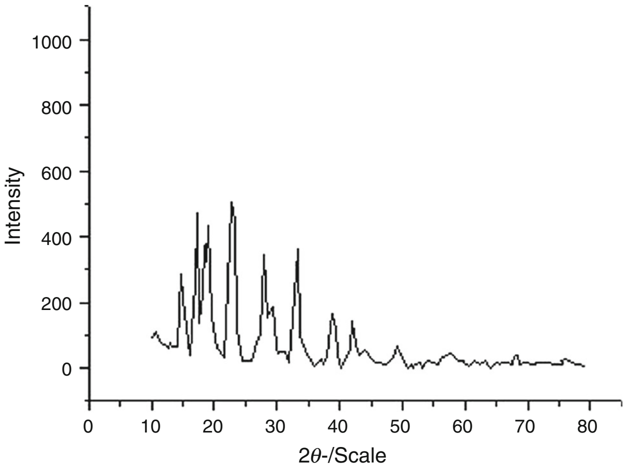

Fig. 7 Powder XRD of MorphcbmH

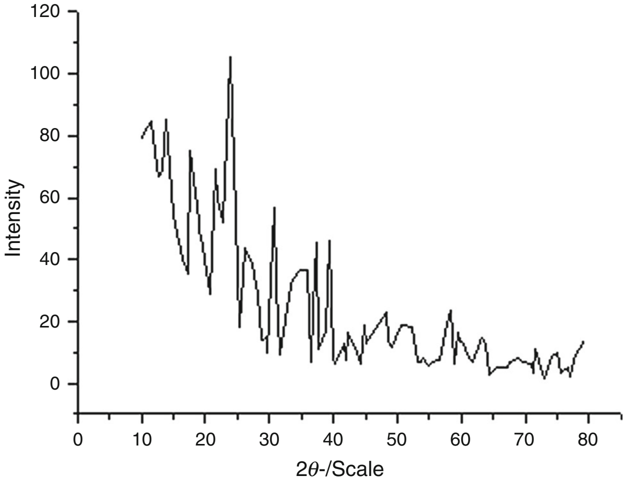

Fig. 8 Powder XRD of $Zn(MorphcbmH)_2Cl_2$

Cyclic voltammetric study

Figures 9–11 show cyclic voltammograms of MorphcbmH, $Cu(MorphcbmH)_2Cl_2$ and $Zn(MorphcbmH)_2(NO_3)_2$. CV data of MorphcbmH ligand revealed a reversible couple

Table 3 XRD data of Morpholinecarbamic acid

Morpholinecarbamic acid					
Sr. no.	d Spacing	2*θ*	Relative intensity/%	FWHM	Dp/nm
1.	3.924	22.656	50.22	0.1476	10.06
2.	5.147	17.227	46.89	0.1968	7.44
3.	4.653	19.072	43.20	0.0984	14.93
4.	4.839	18.331	37.35	0.0984	14.92
5.	2.697	33.217	36.41	0.1968	7.68
6.	3.193	27.939	34.54	0.1968	7.59

Table 4 XRD data of Cu(MorphcbmH)$_2$Cl$_2$ and Cu(MorphcbmH)$_2$(CH$_3$COO)$_2$

Cu(MorphcbmH)$_2$Cl$_2$						Cu(MorphcbmH)$_2$(CH$_3$COO)$_2$					
Sr. no.	d Spacing	2*θ*	Relative intensity/%	FWHM	Dp/nm	Sr. no.	d Spacing	2*θ*	Relative intensity/%	FWHM	Dp/nm
1.	2.032	44.572	14.29	0.1476	10.61	1.	5.529	16.029	93.82	0.344	4.24
2.	1.983	45.734	12.72	0.1476	10.66	2.	3.305	26.973	70.19	0.196	7.58
3.	2.072	43.678	12.11	0.0984	15.87	3.	4.757	18.651	49.99	0.295	4.97
4.	2.148	42.054	10.77	0.3936	3.94	4.	3.979	22.342	49.15	0.246	6.00
5.	1.960	46.264	9.95	0.1800	8.75	5.	2.764	32.386	42.51	0.196	7.70
6.	1.857	49.057	9.49	0.3936	4.04	6.	3.696	24.077	37.19	0.393	3.77

Table 5 XRD Data of Zn(MorphcbmH)$_2$Cl$_2$ and Zn(MorphcbmH)$_2$(NO$_3$)$_2$

Zn(MorphcbmH)$_2$Cl$_2$						Zn(MorphcbmH)$_2$(NO$_3$)$_2$					
Sr. no.	d Spacing	2*θ*	Relative intensity/%	FWHM	Dp/nm	Sr. no.	d Spacing	2*θ*	Relative intensity/%	FWHM	Dp/nm
1.	3.734	23.830	100	0.2952	5.03	1.	4.435	20.001	69.2	0.020	76.26
2.	6.399	13.839	80.91	0.0984	14.93	2.	4.067	21.835	100	0.025	60.37
3.	7.708	11.479	80.23	0.0984	14.93	3.	3.787	23.469	54.7	0.015	103.5
4.	8.160	10.842	78.37	0.2952	4.94	4.	3.622	24.554	53.6	0.014	111.46
5.	5.000	17.735	71.21	0.1968	7.45	5.	3.356	26.538	53.0	0.012	131.72
6.	4.123	21.552	65.44	0.2460	6.01	6.	3.188	27.957	49.4	0.011	136.69

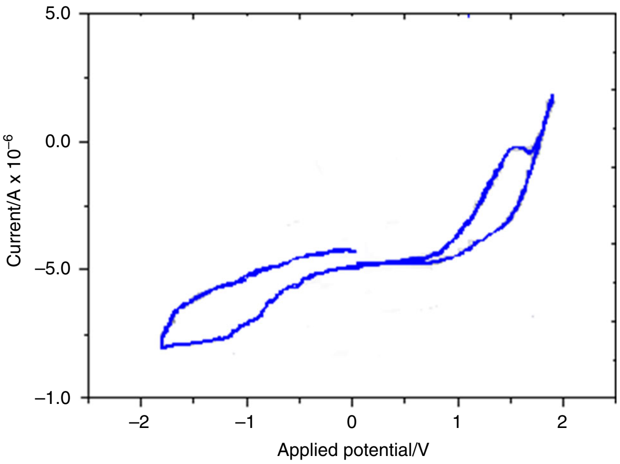

Fig. 9 Cyclic Voltammogram of MorphcpmH

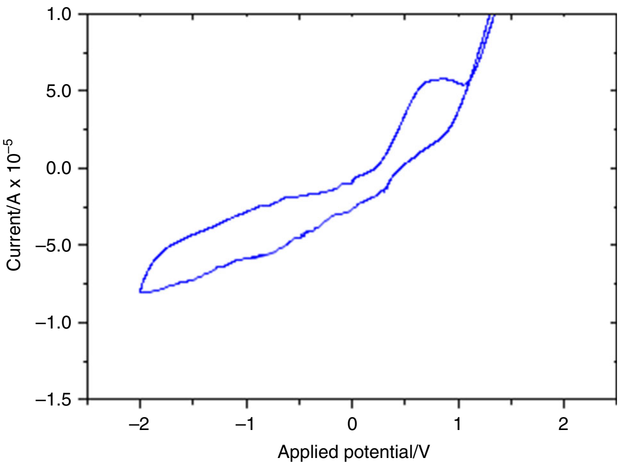

Fig. 10 Cyclic Voltammogram of Cu(MorphcpmH)$_2$Cl$_2$

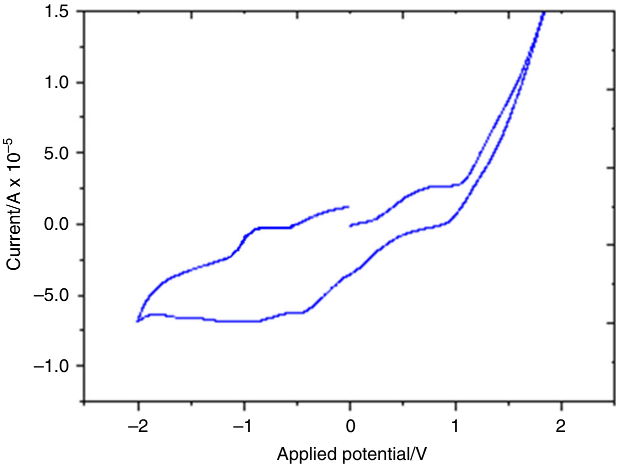

Fig. 11 Cyclic Voltammogram of $Zn(MorphcpmH)_2(NO_3)_2$

with $E_{pa} = 1.50$ V and $E_{pc} = 1.30$ V, $\Delta E = 0.20$ V. Corresponding I_{pa} and I_{pc} values are 4 and 3.6 A, respectively, with $I_{pa}/I_{pc} = 1.11$. The complexes $Cu(MorphcbmH)_2X_2$ ($X = Cl, ClO_4, NO_3$) show well-defined redox process corresponding to the formation of the Cu(II)/Cu(III) couple with anodic peak in the range $E_{pa} = 0.53$–0.65 V and the associated cathodic peak in range $E_{pc} = 0.75$–0.88 V. This couple is found to be reversible with $\Delta E = -0.23$ to -0.19 V and the ratio of anodic to cathodic peak currents $I_{pa}/I_{pc} = 0.75$–1.0 corresponding to a simple one-electron process [21].

Cyclic voltametric measurements for complexes of zinc(II), viz. $Zn(MorphcbmH)_2X_2$ ($X = Cl, ClO_4, NO_3, CH_3COO$ and $X_2 = SO_4$) gave: two anodic waves lying in potential range between E_{pa} = (i) 0.63–0.90 V, (ii) −0.68 to −0.62 V and two cathodic waves lying in potential range between E_{pc} = (i) 0.77–0.93 V, (ii) −1.10 to −0.40 V. Respective ΔEs lie in the range (i) −0.30 to −0.03 V and (ii) −0.28 to 0.44 V with corresponding I_{pa}/I_{pc} = (i) 0.82–1 and (ii) 0.83–0.96. Data of CV study of Zn(II) complexes revealed two cathodic reduction peaks, which are attributed to reduction of Zn(II) → Zn(I) and Zn(I) → Zn(0), respectively, while two anodic oxidation peaks are attributed to oxidation of Zn(0) → Zn(I) and Zn(I) → Zn(II), respectively, indicating reversible one-electron processes. Ratio of I_{pa}/I_{pc} for two reduction as well as two oxidation processes exhibited involvement of one-electron change. Range of potential values of copper(II) and zinc(II) complexes is well in agreement with that of the literature data [22].

Thermal studies

TG curve of free ligand, MorphcbmH (Fig. 12a), shows it to be stable up to 60 °C. It exhibits single-step 100 % decomposition without leaving any residue in the crucible. DSC curves have revealed an endothermic peak at 83 °C (Fig. 12b). This is ascribed to sublimation followed by decomposition to volatile products such as amine, morpholine and carbon dioxide. Endothermic degradation of MorphcbmH ligand is analogous to that for 4-methylpiperazine-1-carbodithioc acid (4-MPipzcdtH) [23]. A total mass loss of 100 % in temperature range of 60–140 °C is in agreement with decomposition path for free MorphcbmH ligand (Eq. 3).

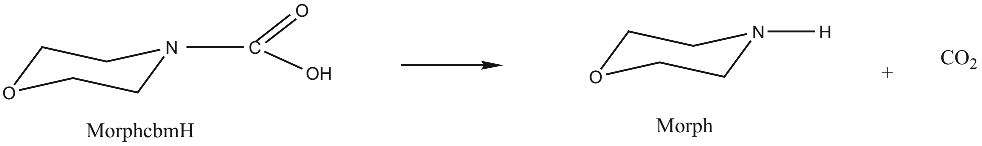

(3)

Decomposition of MorphcbmH

Thermal decomposition of $Cu(MorphcbmH)_2Cl_2$ complex follows four-step pathway (Fig. 12c). First step occurs between 40 and 70 °C with mass loss of 9.12 % corresponding to loss of one mole of hydrochloric acid (Table 6). Second step occurs between 70 and 160 °C with mass loss of 9.15 % due to loss of another mole of hydrochloric acid. Third step involves evolution of carbon dioxide along with one mole of morpholine in temperature range 160–355 °C with 32.95 % mass loss. The fourth step occurs at a temperature of 470–670 °C with mass loss of 29.00 % which corresponds to evolution of one mole of carbon monoxide and amine, i.e., morpholine leaving residual species CuO having 20.05 mass percent. DSC curve of complex exhibits three exothermic peaks at temperatures 43, 157 and 290 °C for first, second and third steps, respectively (Fig. 12d).

That $Cu(MorphcbmH)_2$ was first-stage intermediate of thermal decomposition of $[Cu(MorphcbmH)_2]Cl_2$ at 157 °C has been supported by measuring the FTIR of residue species. This has been done by stopping the heating, cooling the residue and measuring its FTIR. FTIR spectrum of proposed species, i.e., Cu(MorphcbmH)$_2$, exhibited peculiar vibrational modes at 1628, 1450, 657 and 418 cm^{-1} due to characteristic absorptions of ν(CO$_2$), ν(C=N) of NCO$_2$, δ(NCO$_2$) and ν(Cu–O) moieties of MorphcbmH ligand, respectively [8, 10, 24] (Fig. 13).

Thermal decomposition of Cu(MorphcbmH)$_2$(ClO$_4$)$_2$ occurs in three steps (Fig. 12e). First step involves a mass loss of 24.50 % at a temperature of 40–160 °C which may correspond to loss of four moles of O$_2$ (oxidation/reduction process). Elimination of two moles of hydrochloric acid and two moles of amine, i.e., morpholine with total mass loss of 46.95 % at a temperature of 160–345 °C, occurs in second step, while third step occurs at a temperature of 345–605 °C with mass loss of 13.98 % corresponding to elimination of one mole each of CO$_2$ and CO. Mass percent 15.17 % remained as CuO residue (Table 6). DSC curve shows an endothermic peak at 136 °C for first step and two exothermic peaks at 221 and 370 °C for second and third steps, respectively (Fig. 12f). An intramolecular solid phase redox reaction has been proposed to be responsible for appearance of endothermic peak at 136 °C most plausibly attributed to simultaneous presence of both oxidizing (perchlorate) and reducing (morpholine) moieties in a same complex molecule [25]. Final TG residue, CuO was cooled, collected and estimated for copper by EDTA titration. CuO Analysis found: Cu 79.41 %; Calculated: 79.87 %.

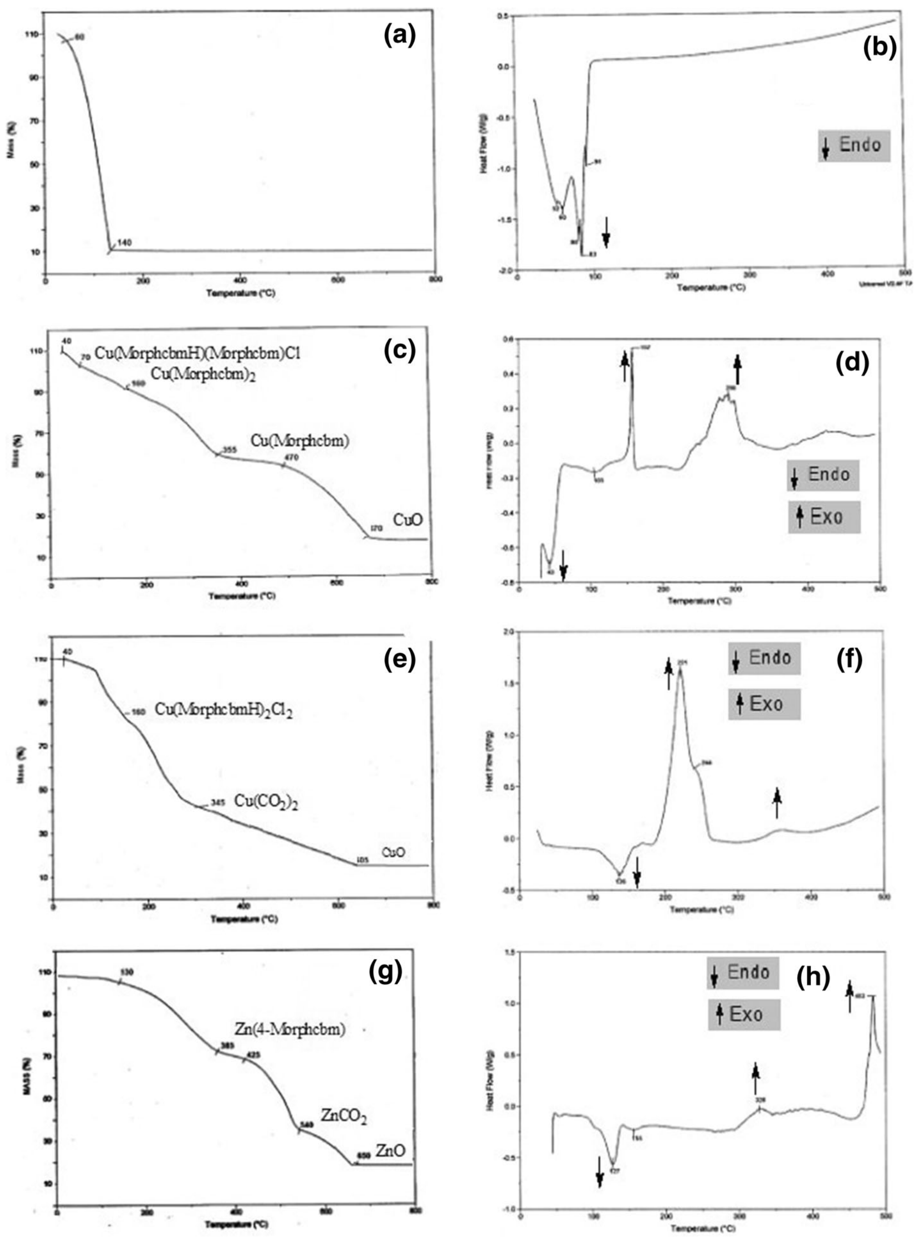

Fig. 12 TG/DSC curves of: **a**, **b** MorphcbmH; **c**, **d** Cu(MorphcbmH)$_2$Cl$_2$; **e**, **f** Cu(MorphcbmH)$_2$(ClO$_4$)$_2$; **g**, **h** Zn(MorphcbmH)$_2$Cl$_2$; **i**, **j** Zn(MorphcbmH)$_2$(ClO$_4$)$_2$; **k**, **l** Zn(MorphcbmH)$_2$(NO$_3$)$_2$ and **m**, **n** Zn(MorphcbmH)$_2$(CH$_3$COO)$_2$

Fig. 12 continued

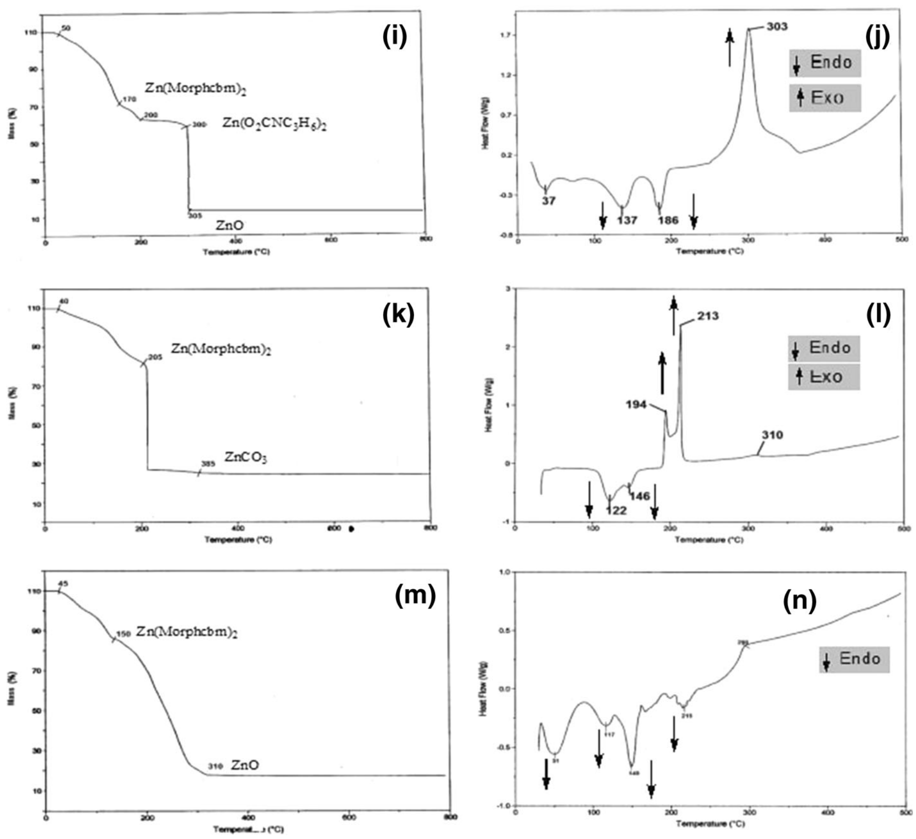

TG/DSC curve of Zn(MorphcbmH)$_2$Cl$_2$ complex (Fig. 12g, h) shows that it has decomposed in three stages. First stage involves elimination of two moles of hydrochloric acid and one mole of morpholine at a temperature of 130–385 °C with mass loss of 40.07 %. Second step occurs at a temperature of 425–540 °C with mass loss of 32.95 % corresponding to loss one mole each of morpholine and carbon dioxide. Last step involves elimination of carbon monoxide molecule with a mass loss of 7.25 % between 540 and 650 °C leaving ZnO as final residue with 20.06 mass percent. DSC curve of complex exhibits one endothermic and one exothermic peak at 127 and 328 °C, respectively, for first step and one exothermic peak at 483 °C for second step (Table 6).

Thermal decomposition of Zn(MorphcbmH)$_2$(ClO$_4$)$_2$ (Fig. 12i) occurs in three steps. First step involves mass loss of 38.30 % at a temperature of 50–170 °C corresponding to loss of two moles of perchloric acid. Elimination (oxidative/reductive: since oxidation process is not independent of reduction process) of one mole of oxygen and one mole of ethylene with a mass loss of 11.50 % at a temperature of 200–300 °C occurs in second step. While the third step occurring at temperature of 300–305 °C with a mass loss of 35 % corresponding to elimination of one mole of CO$_2$, one mole of CO, one mole of nitrogen and three moles of ethylene corresponds well with oxidative decomposition of the intermediate to yield ZnO (15.41 %) as final residue. DSC curve (Fig. 12j) exhibits two endothermic peaks at 137 and 186 °C for first and second steps, respectively, while third step exhibits exothermic peak at 303 °C.

The fact that ZnO was final residue of thermal decomposition of [Zn(4-MorphcbmH)$_2$](ClO$_4$)$_2$ has been inferred from its PXRD pattern (Fig. 14). PXRD pattern exhibited peaks at 2θ values of 31.74°, 34.37°, 36.20°, 47.45°, 56.55°, 62.80° and 67.96° corresponding to planes (100), (002), (101), (102), (110), (103) and (112), respectively. Similar PXRD pattern for ZnO has earlier been reported in the literature [26].

TG/DSC curves of Zn(MorphcbmH)$_2$(NO$_3$)$_2$ and Zn(MorphcbmH)$_2$(CH$_3$COO)$_2$ complexes show them to decompose in two steps (Table 6). The first step involving elimination of two moles of nitric acid and two moles of acetic acid at a temperature of 40–205 and 45–150 °C with mass loss of 28 % and 27 %, respectively(Fig. 12k, m). The second step occurs at a temperature of 205–385 °C with mass loss of 44.40 % corresponding to decomposition of intermediate to loss of one mole of carbon monoxide and two moles of amine, i.e., morpholine in former complex, while in latter complex, it occurs at a temperature of 150–310 °C with mass loss of 55 % corresponding to loss two moles of amine, i.e., morpholine, one mole of carbon

Table 6 Thermal decomposition data of MorphcbmH and its complexes with copper(II) and zinc(II)

Sr. no.	Compound Mol. Wt.	Sample mass/ mg	Initial Dec. Temp/°C	Stages of Dec.	TG Temp./ °C	Mass loss %/ Mol. Wt.		Theor. mass left/% Mol Wt.	Species lost	Species formed	DSC Peak/°C	Nature
						Exp.	Theo.					
1.	MorphcbmH131	25	60	1st	60–140	100 (131)	100 (131)	0 0	CO_2+ 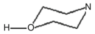		83	Endo
2.	Cu(MorphcbmH)$_2$Cl$_2$-396.5	12	40	1st	40–70	9.12 (36.14)	9.21 (36.50)	90.79 (359.52)	HCl	Cu(MorphcbmH)(MorphcbmH)Cl	43	Endo
				2nd	70–160	9.15 (36.27)	9.21 (36.5)	81.58 (323.05)	HCl	Cu(MorphcbmH)$_2$	157	Exo
				3rd	160–355	32.95	32.78	48.80	CO_2 +	Cu(MorphcbmH)	290	Exo
				4th	470-670	(130.68) 29.00 (114.98)	(130) 28.75 (114)	(193.24) 20.05 (79.39)	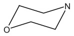 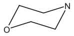 +CO	CuO	–	
3.	Zn(MorphcbmH)$_2$Cl$_2$-398	6.6	40	1st	130–385	40.07 (158.9)	40.10 (159)	59.9 (238.40)	2 HCl+ 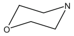	Zn(4-MorphcbmH)	127,328	Endo, Exo
				2nd	425–540	32.95 (130.68)	32.78 (130)	27.12 (107.93)	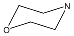 +CO_2	ZnCO$_2$	483	Exo
				3rd	540–650	7.25 (28.85)	7.06 (28)	20.06 (79.83)	CO	ZnO	–	–
4.	Cu(MorphcbmH)$_2$(ClO$_4$)$_2$ 524.5	1.44	40	1st	40–160	24.50 (128.50)	24.40 (128)	75.60 (396.14)	4O_2	Cu(MorphcbmH)$_2$Cl$_2$	136	Endo
				2nd	160–345	46.95 (246.28)	46.71 (245)	28.89	2 HCl+ 2 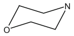	Cu(CO_2)$_2$	221	Exo
				3rd	345–605	13.98 (73.36)	13.72 (72)	15.17 (79.49)	CO_2 + CO	CuO	370	Exo
5.	Zn(MorphcbmH)$_2$(ClO$_4$)$_2$ 526	13	50	1st	50–170	38.30	38.21	61.79	2HClO$_4$	Zn(MorphcbmH)$_2$	137	Endo
				2nd	200–300	(201.46)	(201)	(325.01)	O_2+	ZnO	186	Endo
				3rd	300–305	11.50 (60.49) 35 (184.1)	11.40 (60) 35.98 (184)	50.39 (265.05) 15.41 (81.05)	$CH_2 = CH_2$ 3 $CH_2 = CH_2$ +N_2 + CO_2 +CO		303	Exo

Table 6 continued

Sr. no.	Compound Mol. Wt.	Sample mass/ mg	Initial Dec. Temp/°C	Stages of Dec.	TG Temp./ °C	Mass loss %/ Mol. Wt. Exp.	Mass loss %/ Mol. Wt. Theo.	Theor. mass left/% Mol Wt.	Species lost	Species formed	DSC Peak/°C	Nature
6.	$Zn(MorphcbmH)_2(NO_3)_2$ 451	17	40	1st	40–205	28 (126.28)	27.93 (126)	72.07 (325.03)	$2HNO_3$	$ZnCO_3$	122,147	Endo, Endo
				2nd	205–385	44.40 (200.24)	44.34 (200)	27.73 (125.06)	2  + CO		194,212	Exo, Exo
7.	$Zn(MorphcbmH)_2$ $(CH_3COO)_2$ 445	17	45	1st	45–150	27 (120.15)	26.96 (120)	73.04 (325.02)	2 CH_3COOH	Zn $(MorphcbmH)_2$	51,117, 148	Endo, Endo, Endo
				2nd	150–310	55 (244.75)	54.83 (244)	18.21 (81.03)	2 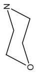 + CO_2 +CO	ZnO	214	Endo

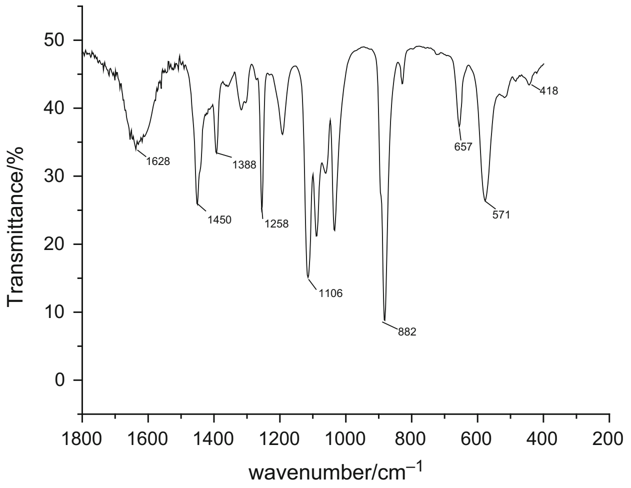

Fig. 13 FTIR spectrum of first-stage intermediate Cu(4-MorphcbmH)$_2$ of thermal decomposition of Cu(4-MorphcbmH)$_2$]Cl$_2$

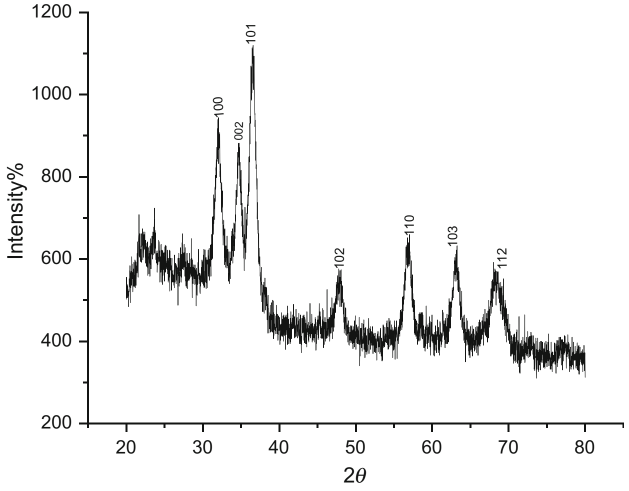

Fig. 14 Powder XRD of final residue (ZnO)

monoxide and one mole of carbon dioxide. Residue left corresponds to $ZnCO_3$ in former case and ZnO in latter case with 27.73 and 18.21 % mass percent, respectively. The DSC curve of $Zn(MorphcbmH)_2(NO_3)_2$(Fig. 12l) shows two endothermic peaks at a temperature of 122 and 147 °C, while second step shows two exothermic peaks at 194 and 212 °C. DSC curve of $Zn(MorphcbmH)_2(CH_3COO)_2$ (Fig. 12n) shows three endothermic peaks at 51, 117 and 148 °C for first step and one endothermic peak at a temperature of 214 °C for second step.

Thermal decomposition patterns for carbamate compounds, viz. $[Zn(MorphcbmH)_2]Cl_2$, $[Zn(MorphcbmH)_2](CH3COO_2)_2$ and $[Zn(MorphcbmH)_2](NO_3)_2$, i.e., with monovalent counter anions, were not observed to be comparable. In these particular cases, the anion effect may most plausibly contribute to a combination of factors related to

Table 7 Effect of MorphcbmH and some of its copper(II) and zinc(II) compounds on lipase activity (μ mol mL^{-1} min^{-1})

Chemical compound	Lipase activity 0 min	Lipase activity 10 min	Lipase activity 30 min	Lipase activity 50 min	Lipase activity 70 min
MorphcbmH	28.58	2.712	0.898	0.564	0.403
$Cu(MorphcbmH)_2Cl_2$	31.86	3.022	0.869	0.464	0.186
$Cu(MorphcbmH)_2(ClO_4)_2$	27.51	2.677	0.865	0.514	0.357
$Cu(MorphcbmH)_2(NO_3)_2$	32.03	3.169	1.043	0.605	0.420
$Zn(MorphcbmH)_2Cl_2$	43.16	4.096	1.362	0.651	0.446
$Zn(MorphcbmH)_2(ClO_4)_2$	48.16	5.070	1.187	0.623	0.341
$Zn(MorphcbmH)_2(NO_3)_2$	34.97	3.458	1.148	0.685	0.044
$Zn(MorphcbmH)_2(CH_3COO)_2$	30.30	3.122	0.901	0.565	0.345
$Zn(MorphcbmH)_2SO_4$	38.41	3.012	1.012	0.563	0.401

crystal lattice, e.g., mismatching of ion size, shape and imbalance of attractive power while TG/DSC curves for $[Zn(4\text{-}MorphcbmH)_2](ClO_4)_2$ and $[Zn(4\text{-}MorphcbmH)_2](NO_3)_2$ have exhibited similar exothermic one and two decomposition steps with single broad exotherm for former and two sharp exotherms for latter complex. However, final residue percentage of 15.41 and 27.73 % for two complexes, respectively, as well as of 15.17 % for $[Cu(MorphcbmH)_2](ClO_4)_2$ has revealed non-explosive nature of complexes with perchlorate and nitrate as counter anions.

It has been observed that for TG/DSC patterns for the complexes under investigation experimental percent mass loss matches with the corresponding theoretical percent mass loss (Table 6) for their various stages of thermal decomposition which supports present thermal decomposition pattern is in relevance to the literature reports [23].

Lipase enzyme activity

Compounds under study were also tested for the lipase enzyme (steapsin) activity at different incubation times between 0 and 70 min. The activity of the lipase enzyme is maximum at zero minute (27.51–48.16 μmol mL^{-1} min^{-1}). When we add one milligram of compound to the lipase enzyme, then after 10 min its activity decreases (2.677–5.070 μmol mL^{-1} min^{-1}). After 30, 50 and 70 min, the lipase enzyme activity further decreases as 0.865–1.362, 0.464–0.685 and 0.044–0.446 μmol mL^{-1} min^{-1}, respectively (Table 7). This shows that in the presence of newly synthesized compounds, the activity of the lipase enzyme decreases with increase in time. Hence, MorphcbmH and its copper(II) and zinc(II) compounds retard the lipase enzyme activity with time due to fact that carbamate compounds block the active site of the lipase enzyme. Lipase inhibition activity is used for designing drugs for the treatment of obesity and problems of acne.

Conclusions

Morpholinecarbamic acid and its copper(II) and zinc(II) complexes were synthesized and investigated by FTIR, fluorescence, UV–visible and ^{1}H NMR spectroscopy, magnetic studies which support four coordination around copper(II) and zinc(II). Thermal study of MorphcbmH and its complexes indicated their low thermal stability, IDT values 40–80 °C with the exception of $Zn(MorphcbmH)Cl_2$ (IDT = 130 °C). TG curves exhibit two or more than two steps of decomposition patterns. The final product of thermal decomposition is MO or MCO_3 (M = Cu, Zn). All complexes gave increase in lipase enzyme inhibition activity (48.16–0.044 μmol mL^{-1} min^{-1}) with increase in time due to their ability to block the active site of the lipase enzyme.

References

1. Ali RMA, Mohsen R, Parisa N. Solvent-free preparation of primary carbamates. Turk J Chem. 2006;30:269–76.
2. Dibenedetto A, Aresta M, Fragale C, Narracci M. Reaction of silylalkylmono-and silylalkyldi-amines with carbon dioxide: evidence of formation of inter-and intramolecular ammonium carbamates and their conversion into organic carbamate of industrial interest under carbon dioxide catalysis. Green Chem. 2002;4:439–43.
3. Gupte SP, Shivarkar AB, Chaudhari RV. Carbamate synthesis by solid-base catalyzed reaction of disubstituted ureas and carbonates. J Chem Soc Chem Commun. 2001;24:2620–1.
4. Thompson A. Pest control on field vegetables threatened by the loss of organophosphorus (OP) and carbamate insecticides. Pestic Outlook. 2002;13:84–6.
5. Martin LL, Davis L, Klein JT, Nemoto P, Olsen GE, Bores GM, Camacho F, Petko WW, Rush DK, Selk D, Smith CP, Vargas HM, Wilson JT, Effland RC, Fink DM. Synthesis and preliminary structure-activity relationships of 1-[(3-fluoro-4-pyridinyl)-amino]-3-methyl-1H-indol-5-yl methyl carbamate (P10358), a novel acetylcholinesterase inhibitor. Bioorg Med Chem Lett. 1997;7:157–62.

6. Daly NJ, Ziolkowski F. The thermal decompositions of carbamates. IV. The ethyl *N*-methyl-carbamate system. Int J Chem Kinet. 1980;12:241–52.
7. Kim CK, Kim DJ, Zhang H, Hsieh Y-H, Lee B-S, Lee HW, Kim CK. Substituent effects on the gas-phase pyrolyses of 2-substituted ethyl *N*,*N*-dialkylcarbamates: a theoretical study. Bull Korean Chem Soc. 2007;28:1031–4.
8. Kalia SB, Sankhyan P, Puri R, Christopher J. Thermoanalytical behaviour of carbaryl and its copper(II) and zinc(II) complexes. J Therm Anal Calorim. 2012;107(2):597–605.
9. Kalia SB, Kumar D, Sharma M, Christopher J. Physico-chemical investigations and thermal degradation behaviour of 4-ethylpiperazine-1-carbodithioic acid complexes of cobalt(II). J Therm Anal Calorim. 2015;120:1099–106.
10. Amico DBL, Calderazzo F, Labella L, Marchetti F, Pampatoni G. Converting carbon dioxide into carbamato derivatives. Chem Rev. 2003;103:3857–97.
11. Chisholm MH, Extine M. Reactions of transition metal-nitrogen σ-bonds. 3. Early transition metal *N*,*N*-dimethylcarbamates. Preparation, properties and carbon dioxide exchange reactions. J Am Chem Soc. 1977;99:782–92.
12. Yan H, Zhong C, Zhou Y, Zhang H. Synthesis and luminescent properties of novel Cu(II), Zn(II) polymeric complexes based on 1,10-phenanthroline and biphenyl groups. J Chem Sci. 2009; 121:407–12.
13. Onal Z, Zengin H, Sonmez M. Synthesis, characterization, and photoluminescence properties of Cu(II), Co(II), Ni(II), and Zn(II) complexes of *N*-aminopyrimidine-2-thione. Turk J Chem. 2011;35:905–14.
14. Nikolov GS. Correlations between spectroscopic data por diethyldithiocarbamate complexes. Inorg Nucl Chem Lett. 1971;7: 1213–7.
15. Kumar S, Kaushik NK. Titanium(IV) and zirconium(IV) dithiocarbamates. Synth React Inorg Met Org Chem. 1982;12(2):159.
16. Hofmann H. Adv Nanomater 2011;18–40.
17. Tang Y, Kassel SW, Zakharov NL, Rheingold AL, Kemp AP. Insertion reactions of carbon dioxide into Zn–N bonds: syntheses and structures of tetrameric and dimeric alkylzinc carbamato complexes. Inorg Chem. 2005;44:359.
18. Goldstein GI, Newbury DE, Echlin P, Joy DC, Fiori C, Lifshin E. Scanning electron microscopy and X-ray microanalysis. New York: Plenum Press; 1981.
19. Tomar R, Sharma P, Sharma P, Tomar R. Studies on the crystallographic changes in an analogue of aluminosilicate mineral Muscovite on sorption of UO_2^{2+}, Th^{4+} & Ru^{3+}. Ind J Chem. 2006;45(A):1400–4.
20. Rafel I, Heidi ES, Mathias B, Marco K, Peter E. Crystalline complexes of agriculturally active organic compounds. US Patent App. 20100113543; 2010.
21. Shirin Z, Mukherjee RM. Stable cyclohexadienyl complexes of ruthenium in a piano stool geometry containing a tridentate nitrogen donor ligand. First structural characterization of the (5-cyanocyclohexadienyl)ruthenium(II) complex and spectroelectrochemical correlation. Polyhedron. 1992;11:2625.
22. Raman N, Ravichandran S, Thangaraja C. Copper(II), cobalt(II), nickel(II) and zinc(II) complexes of Schiff base derived from benzil-2,4-dinitrophenylhydrazone with aniline. J Chem Sci. 2004;116(4):215–9.
23. Kalia SB, Kaushal G, Lumba K. Priyanka. Thermoanalytical investigations of 4-methylpiperazine-1-carbodithioic acid ligand and its iron(III), copper(II) and zinc(II) complexes. J Therm Anal Calorim. 2008;91(2):609–13.
24. Yesilkaynak T. 2-Chloro-*N*-((5-chloropyridine-2-yl)carbamothioyl)benzamide and its Co(II), Ni(II) and Cu(II) metal complexes Synthesis, characterization, thermal decomposition, electrochemical behavior and antioxidant activity. J Therm Anal Calorim. 2016;124:1029–37.
25. Singh G, Shrimal AK, Kapoor IPS, Singh CP, Kumar D, Manan SM. Kinetics of thermolysis of some transition metal perchlorate complexes with 1,6-diaminohexane ligand. J Therm Anal Calorim. 2011;103(1):149–55.
26. Malecka B, Lacz A, Drozdz E, Malecki A. Thermal decomposition of d-metal nitrates supported on alumina. J Therm Anal Calorim. 2015;119:1053–61.